Microporous and Mesoporous Materials 328 (2021) 111505

Contents lists available at ScienceDirect

Microporous and Mesoporous Materials

journal homepage: www.elsevier.com/locate/micromeso

Ultrastable porous organic/inorganic polymers based on polyhedral oligomeric silsesquioxane (POSS) hybrids exhibiting high performance for thermal property and energy storage

Mohamed Gamal Mohamed [a,b], Tharwat Hassan Mansoure [b], Yasuno Takashi [a], Maha Mohamed Samy [a], Tao Chen [c], Shiao-Wei Kuo [a,d,*]

[a] Department of Materials and Optoelectronic Science, Center of Crystal Research, National Sun Yat-Sen University, Kaohsiung, 80424, Taiwan
[b] Chemistry Department, Faculty of Science, Assiut University, Assiut, 71516, Egypt
[c] Ningbo Institute of Material Technology and Engineering, Chinese Academy of Science, Ningbo, 315201, China
[d] Department of Medicinal and Applied Chemistry, Kaohsiung Medical University, Kaohsiung, 807, Taiwan

ARTICLE INFO

Keywords:
Porous organic-inorganic polymers
POSS
Anthraquinone
Heck coupling reaction
Energy storage

ABSTRACT

In our work, we have been synthesized two-hybrid porous organic-inorganic microporous polymers (POIPs) through a simple and friendly Heck coupling reaction at a moderate temperature of cubic octavinylsilsesquioxane (OVS) with brominated fluorene (F–Br_2) and anthraquinone (A-Br_2); respectively, to afford POSS-F-POIP and POSS-A-POIP. FTIR, solid-state ^{13}C, and ^{29}Si NMR spectroscopy analyses were carried out to confirm the chemical structures of these POIP materials and the presence of POSS units within their framework. TGA measurements revealed that POSS-A-POIP possesses high thermal stability (T_{d10}: 600 °C, and char yield: 83 wt%) due to the presence of rigid anthraquinone and POSS units. Furthermore, POSS-A-POIP features pseudocapacitor with high symmetry and high specific capacitance of 152.5 F g^{-1} at 0.5 A g^{-1} when compared with the POSS-F-POIP (36.2 F g^{-1} at 0.5 A g^{-1}). The excellent energy storage performance of POSS-A-POIP could be attributed to the Faradaic reaction of anthraquinone and the π-conjugated system.

1. Introduction

Porous organic polymers (POPs) are interesting materials because of their unique features including excellent chemical resistance, low regeneration energy, low density, high thermal stability, facile preparation, ease post functionalization and modification, high surface area, and tunable porosity [1–10]. The preparation of POPs was carried out and reported by using different synthetic methodologies such as Heck crosslinking coupling, Friedel-Graft's reaction, $FeCl_3$ oxidative polymerization, Suzuki coupling reactions, Buchwald–Hartwig (BH) coupling, Schiff-base condensation, Yamamoto reaction, Sonogashira-Hagihara coupling reaction [11–25]. These interesting materials have been used in some applications including enantioseparation, energy storage, drug delivery, chemical sensing for metals ions, separation analyses, dyes removing from water, gas adsorption and conversion, lithium, and sodium ions batteries, nanofiltration, hydrogen production (H_2) from water, photocatalysis, light-harvesting, iodine adsorption and optoelectronic devices [26–43]. Nowadays, the preparation of porous hybrid polymers with high surface area, optical transparency, high thermal and mechanical strength based on polyhedral oligomeric silsesquioxanes (POSS) have been synthesized widely and these materials have been widely applied in catalysis, aerospace, microelectronics, chemical sensing, water treatment, biomedicine, iodine capture and so on [44–55]. Cubic octavinylsilsesquioxanes (OVS) are a class of silsesquioxane cages with an empirical formula ($RSiO_{1.5}$), and a diameter in the range of 1–3 nm [56–62]. There are many examples for the preparation of porous polymers by using OVS as a building unit with high BET specific surface area, outstanding thermal stability, tunable morphology, and fluorescence properties were reported and done by many groups by using Heck coupling reaction [44–55,63–65]. There is enormous demand for clean and low-price environmentally friendly energy storage devices with high performance, due to the prosperity in manufacturing of wearable and portable electronic devices [66–75]. For high energy storage devices, very high power and/or energy density,

* Corresponding author. Department of Materials and Optoelectronic Science, Center of Crystal Research, National Sun Yat-Sen University, Kaohsiung, 80424, Taiwan.
E-mail address: kuosw@faculty.nsysu.edu.tw (S.-W. Kuo).

https://doi.org/10.1016/j.micromeso.2021.111505
Received 31 May 2021; Received in revised form 11 October 2021; Accepted 13 October 2021
Available online 16 October 2021
1387-1811/

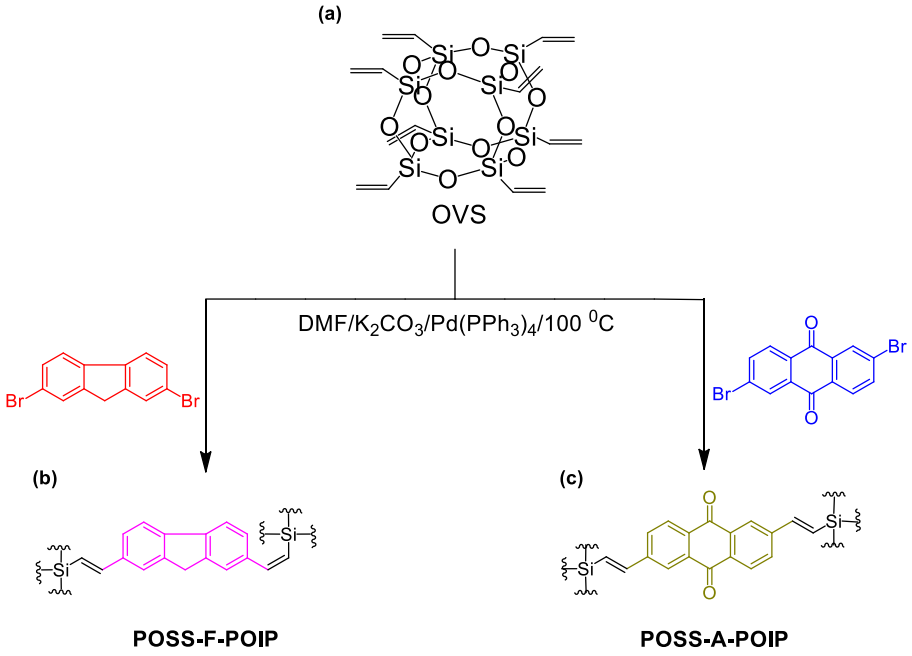

Scheme 1. Synthesis of (b) POSS-F-POIP and (c) POSS-A-POIP from (a) OVS through Heck coupling reaction.

excellent safety features, use of abundant elements, long durability, and prolonged cycle life are the most important parameters. Among the high-performance energy storage devices, Supercapacitors which characterized by high power density, remarkable safety, and long-life span which may exceed 10^6 cycles and relatively low cost [72–75]. However, the lower energy density of supercapacitors (<10 Wh kg^{-1}) than those of batteries were severely hindered their applications [76]. The energy density of supercapacitors could be improved by incorporating redox moieties into carbonaceous materials which provides a chance to merge the merits of the electrical double-layer capacitor (EDLC) and pseudocapacitor mechanisms [77,78]. For instance, anthraquinone-decorated graphene hydrogel [79], heteroatom-doped carbon materials [80,81], transition metal oxide dispersed nitrogen-doped porous carbons [82], introducing of 2,6-diaminoanthraquinone (DAAQ) moieties as redox-active into the 2D COF [70], graphene oxide (GO) [83,84] and polyacrylonitrile/POSS derived carbon nanofibers (CNFs) [85] have been reported. Though the use of OVS, fluorene and anthraquinone based on hybrid porous polymers for energy storage has not been discussed until now. In this work, we have been successfully synthesized hybrid organic-inorganic microporous polymers through the Heck reaction of octavinylsilsesquioxane as a building unit with brominated fluorene (F–Br_2) and anthraquinone (A-Br_2) in the solution state to afford POSS-F-POIP and POSS-A-POIP as displayed in Scheme 1. Their chemical structures of corresponding monomers and polymers, their thermal stability, texture porosity, morphology, CO_2 capture, and electrochemical performance were discussed in detail.

2. Experimental section

2.1. Materials

Octavinylsilsesquioxane (OVS) and potassium carbonate (K_2CO_3) were ordered from Alfa Aesar. Tetrahydrofuran (THF), N,N-dimethylformamide (DMF), methanol (MeOH), and acetone were obtained from Acros. Triethylamine (Et_3N) and tetrakis(triphenylphosphine) palladium(0) [$Pd(PPh_3)_4$] were purchased from Sigma–Aldrich. DMF was dried over CaH_2 for 24 h. All molecules in this study are not toxic and need to use gloves for safety.

2.2. Synthesis of 2,7-Dibrmo-9H-fluorene (F–Br_2)

In double-necked flask (100 mL) under N_2, 4.00 g of fluorene (24.0 mmol) was soluble in 50 mL of dry $CHCl_3$. Then, 0.134 g of $FeCl_3$ (2.40 mmol) in 40 mL of $CHCl_3$ was added dropwise to the reaction mixture. After that, Br_2 solution (1.29 mL, 25.27 mmol) was dropwise to the mixture at 0 °C and kept the reaction in the dark for 4 h. After completing the reaction, the reaction solution was extracted three times with saturated aqueous $Na_2S_2O_5$. The organic layer was dried over $MgSO_4$ and removed under a vacuum system to afford F–Br_2 as a white powder (7.80 g, 89%). M.p.:165 °C (DSC, Fig. S1). FTIR (KBr, cm^{-1}): 3051, 2922, ^{1}H NMR (500 MHz, $CDCl_3$, δ, ppm, Fig. S2): 3.90 (2H), 7.51 (2H), 7.61 (2H), 7.66 (2H). ^{13}C NMR (125 MHz, $CDCl_3$, δ, ppm, Fig. S3): 145.36, 140.13, 130.98, 128.35, 122.06, 36.69.

2.3. Synthesis of 2,6-dibromoanthraquinone (A-Br_2)

In dry 250 mL flask under N_2 containing acetonitrile (100 mL), $CuBr_2$ (15.63 g, 71.5 mmol), 2,6-diaminoanthraquinone (6.87 g, 28.6 mmol), and *tert*-butyl nitrite (8 mL). The brown solid was formed after refluxing at 80 °C for 12 h. The brown solid was purified by the crystallization in 1,4-dioxane as a solvent to obtain A-Br_2 (7.87 g, 98% yield). M.p.: 285–287 °C (DSC). ^{1}H NMR (500 MHz, $CDCl_3$, δ, ppm, Fig. S4): 8.43 (2H), 8.15 (2H), 7.95 (2H). ^{13}C NMR (125 MHz, $CDCl_3$, δ, ppm, Fig. S5): 179.66, 135.89, 132.97, 130.41, 128.83, 128.68, 127.60.

2.4. Synthesis of POSS- F-POIP and POSS-A-POIP

In two neck flask (100 mL), A mixture of F–Br_2 (0.40 g, 0.126 mmol), or A-Br_2 (0.50 g, 0.136 mmol), OVS (0.40 g, 0.63 mmol), potassium carbonate (1.40 g, 1 mmol) and $Pd(PPh_3)_4$ (0.04 g, 0.0034 mmol) in DMF (30 mL) and then the reaction solution was stirred and heated for 48 h at 120 °C under N_2. After cooling to room temperature, the obtained solid was washed with DMF, THF, acetone, and methanol. Finally, the product was dried in an oven for 24 h at 70 °C under a vacuum environment to get yellow powder (0.30 g, 80%) for POSS-F-POIP and dark green powder (0.43 g, 85%) for POSS-A-POIP.

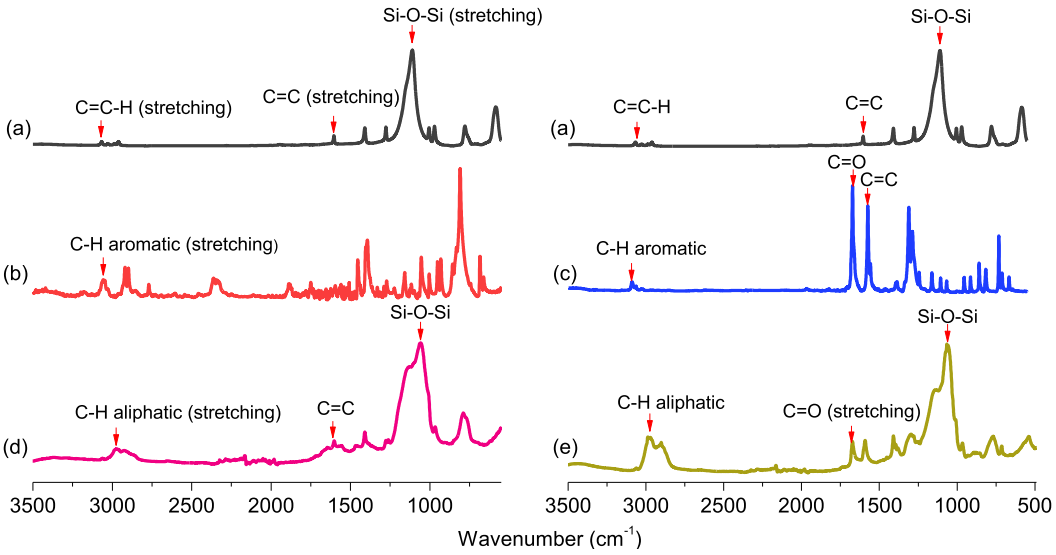

Fig. 1. FTIR analyses of (a) OVS, (b) F–Br_2, (c) A-Br_2, (d) POSS-F-POIP, and (e) POSS-A-POIP.

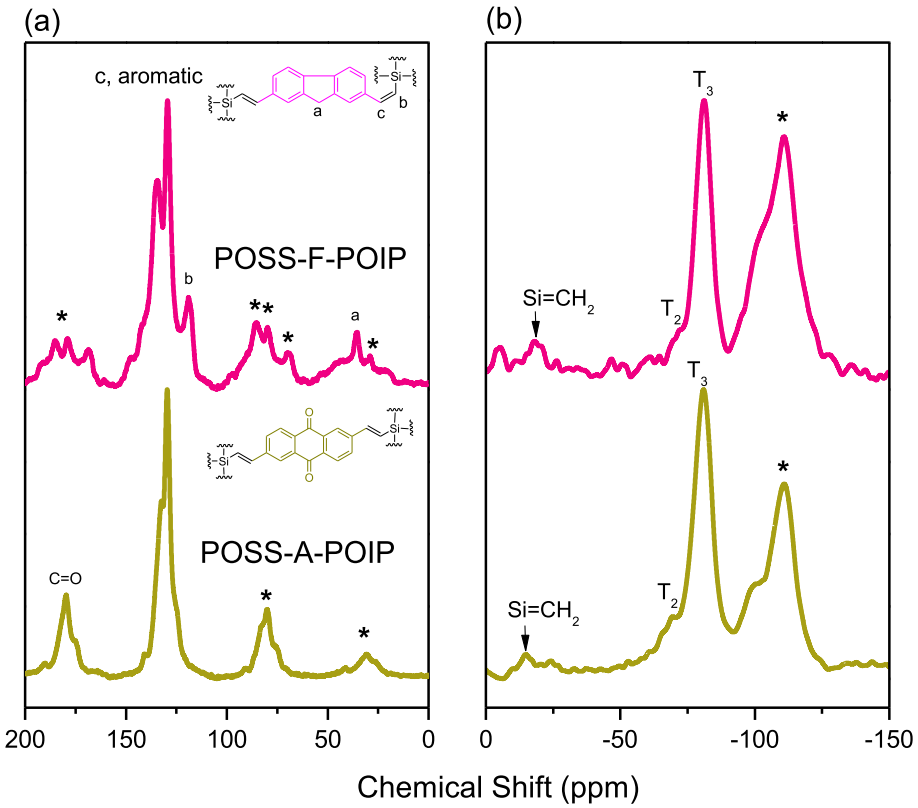

Fig. 2. (a) ^{13}C and (b) ^{29}Si solid-state NMR spectra of POSS-F-POIP and POSS-A-POIP. Asterisks denote spinning sidebands.

3. Results and discussion

Scheme 1 shows the preparation of two types of porous organic-inorganic polymers based on POSS, 9H-fluorene, and anthraquinone (POSS-F-POIP and POSS-A-POIP). Firstly, F–Br_2 was prepared through the reaction of 9H-fluorene with bromine solution in the $CHCl_3$ as solvent at 0 °C (Scheme S1(a)). Secondly, A-Br_2 was synthesized via the reaction of 2,6-diaminoanthraquinone with *tert*-butyl nitrite and $CuBr_2$ in dry acetonitrile at 70 °C (Scheme S1(b)). Thirdly, POSS-F-POIP and POSS-A-POIP were obtained through the Heck coupling reaction of F–Br_2 and A-Br_2 with OVS in anhydrous DMF containing potassium carbonate and $Pd(PPh_3)_4$ as a catalyst for 72 h at 120 °C as shown in Scheme 1. The obtained POSS-F-POIP and POSS-A-POIP were insoluble in THF, DCM, MeOH, DMSO, $CHCl_3$, and acetone. Their chemical structures of the POSS-F-POIP and POSS-A-POIP were carefully confirmed by using different instruments including solid-state ^{13}C and ^{29}Si NMR, and FTIR spectroscopy recorded at 25 °C. As presented in Fig. 1(a), the corresponding absorption bands for the stretching C═C–H, C═C, and Si–O–Si groups in the OVS molecules appeared at 3066, 1600, and 1107 cm^{-1}, respectively. The characteristic absorption bands at

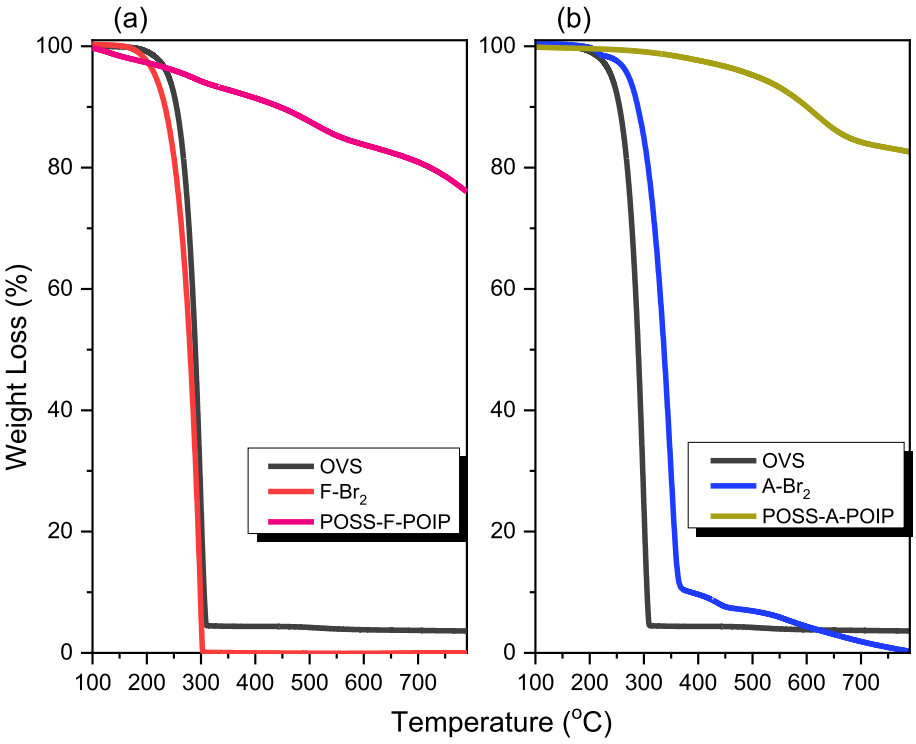

Fig. 3. TGA analyses of (a) OVS, F–Br_2, and POSS-F-POIP and (b) OVS, A-Br_2, and POSS-A-POIP.

3064 and 3081 cm^{-1} corresponding to the C–H aromatic in the F–Br_2 and A-Br_2; respectively (Fig. 1(b) and (c)). As displayed in Fig. 1(d) and (e), the absorption signals in the FTIR profiles of the POSS-F-POIP and POSS-A-POIP were observed in the range 2981–2964 and 1600-1590 cm^{-1} for their stretching aliphatic C–H units and double bonds (C═C). As expected, the absorption bands of the Si–O–Si units in both two porous materials (Fig. 1(d) and (e)) were broader than the stretching vibrations of the Si–O–Si unit in the OVS compound, which is attributed to the formation of cross-linked networks.

As observed in the solid-state ^{13}C NMR of the POSS-F-POIP and POSS-A-POIP (Fig. 2(a)), the signals of the carbon nuclei were located at 148.70-129.19, 134.23, and 118.55 ppm; respectively for the POSS-F-POIP and at 140.70-129.48, 131.84, and 124.45 ppm; respectively for the POSS-A-POIP, which are representing to their aromatic carbons, SiCH═CH and SiCH= CH-Ph units; respectively. The peak at 35.30 ppm in the spectrum of POSS-F-POIP is due to the presence of the CH_2(**a**) unit in the fluorene moiety. In addition, the spectrum of POSS-A-POIP had a carbon signal at 179.96 ppm, representing the C═O groups. Furthermore, the remaining POSS units in both POSS-F-POIP and POSS-A-POIP frameworks were confirmed by using ^{29}Si MAS NMR measurements (Fig. 2(b)). The signals were observed near at −14.46, −69.28, and −80.78 ppm in both samples which are attributed to the Si═CH_2, T_2, and T_3 units in their framework. Taken all spectral analyses, as shown above, they confirmed the successful syntheses of the POSS-F-POIP and POSS-A-POIP framework.

The thermal stability of new POSS-F-POIP and POSS-A-POIP was tested using thermogravimetric analysis under N_2 at 20 °C min^{-1}, as provided in Fig. 3. TGA profiles (Fig. 3(a) and (b)) showed the thermal decomposition temperatures of T_{d5}, T_{d10} with a char yield at 246, 263 °C, and 3.6 wt%; respectively; for OVS. For F–Br_2, they were 215 °C, 233 °C, and 0 wt% respectively; for A-Br_2; they were 272 °C, 289 °C, and 0 wt % respectively. Interestingly, we observed that after crosslinking formation of OVS with F–Br_2 and A-Br_2 through Heck coupling reaction, we found that the thermal stability of the resulting porous materials significantly increased. For example, the values of T_{d5}, T_{d10} and the char yield of POSS-F-POIP were 277 °C, 442 °C, and 76 wt% respectively; for POSS-A-POIP they were 508 °C, 600 °C, and 83 wt%; respectively. Furthermore, the POSS-A-POIP framework displayed higher thermal stability as compared with POSS-F-POIP and the other porous frameworks [48] due to the anthraquinone structure and its high crosslinking density. The thermal stability results (including T_{d5} and T_{d10} and the char yields) of the POSS-F-POIP and POSS-A-POIP were summarized in Table 1.

Table 1
Thermal and porosity properties of POSS-F-POIP and POSS-A-POIP materials.

Materials	T_{d5} (°C)	T_{d10} (°C)	Char yield (wt%)	S_{BET} (m^2 g^{-1})	$S_{Langmuir}$ (m^2 g^{-1})	V_{total} (cm^3 g^{-1})	Pore size (nm)
POSS-F-POIP	277	442	76	452	689	0.80	2.14
POSS-A-POIP	508	600	83	426	651	1.14	2.06

The POSS-F-POIP and POSS-A-POIP are amorphous materials and did not have long-range order character, as revealed in powder X-ray diffraction pattern (Fig. S6) and these results were also observed with other porous POSS-based materials. The observed diffraction peaks near at $2\theta = 22.86°$ in POSS-F-POIP and POSS-A-POIP framework, which also appeared in amorphous silica nanocomposites and participated with the Si–O–Si units. To confirm the porosity properties of the POSS-F-POIP and POSS-A-POIP framework, the N_2 adsorption-desorption analyses were done at 77 K and 1 bar (Fig. 4). Fig. 4(a) and (b) show that the N_2 uptake profiles of the POSS-F-POIP and POSS-A-POIP framework exhibited type I isotherms with some type IV isotherm features according to IUPAC classification. As shown in both isotherms, at low and high relative pressure (P/P_0); POSS-F-POIP and POSS-A-POIP framework had a sharp N_2 uptake due to the presence of mesopores and micropores character within these materials. The S_{BET}, Langmuir surface areas, and total pore volumes of POSS-F-POIP were 452 m^2 g^{-1}, 689 m^2 g^{-1}, and 0.8 cm^3 g^{-1}; respectively (Table 1). While the POSS-A-POIP possesses S_{BET} surface area of 426 m^2 g^{-1}; and Langmuir surface area of 651 m^2 g^{-1} with total pore volumes of 1.14 cm^3 g^{-1} (Table 1). Finally,

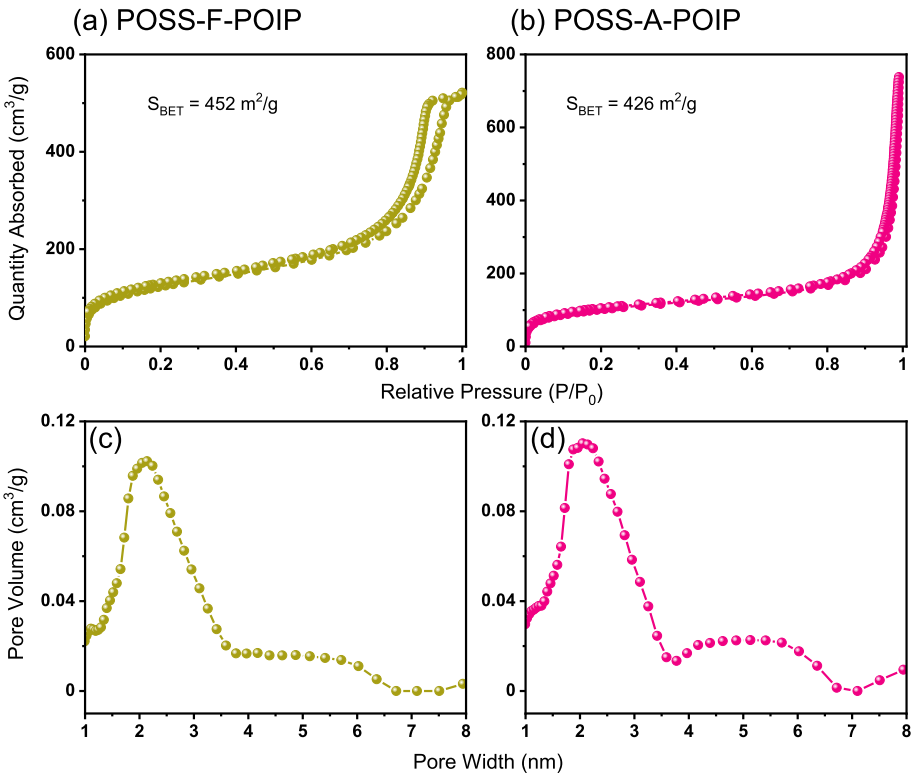

Fig. 4. N_2 isotherms and pore size diameter of POSS-F-POIP (a, c) and POSS-A-POIP (b, d).

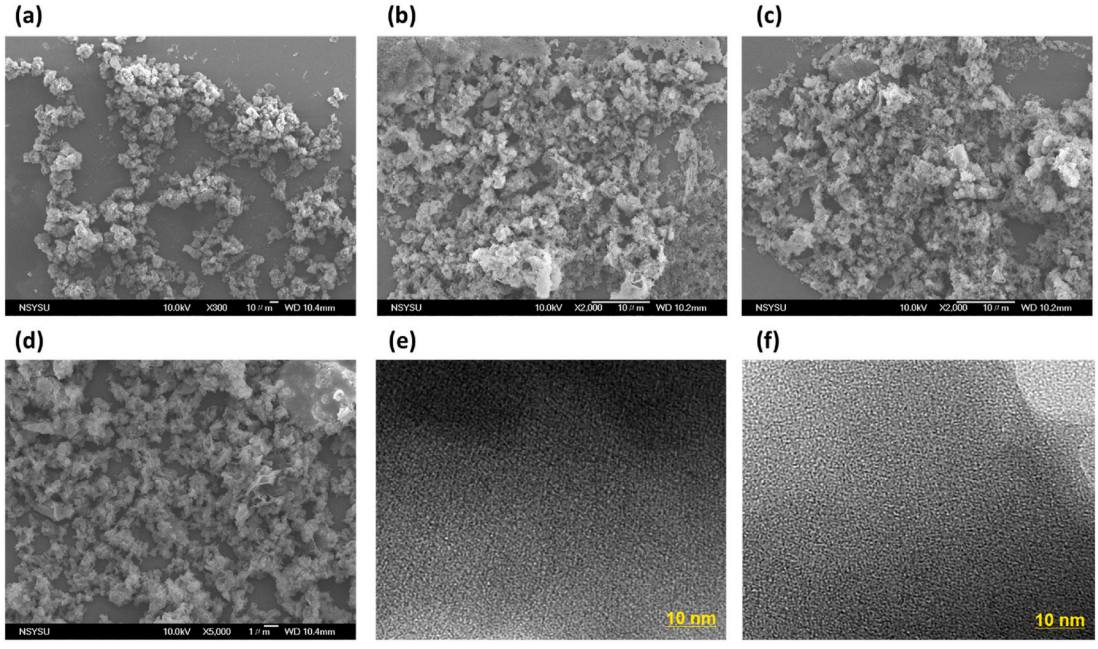

Fig. 5. SEM images of POSS-F-POIP (a and b) and POSS-A-POIP (c and d). TEM images of (e) POSS-F-POIP and (f) POSS-A-POIP.

the pore size diameters of POSS-F-POIP and POSS-A-POIP (Fig. 4(c) and (d)) based on nonlocal density functional theory (NL-DFT) were 2.04 and 2.06 nm; respectively.

FE-SEM and HR-TEM (Fig. 5) were performed to investigate the morphology, ordering, and porosity properties of POSS-F-POIP and POSS-A-POIP. The SEM images of POSS-F-POIP and POSS-A-POIP (Fig. 5 (a)–(d) and Fig. S7) exhibited irregular aggregated small spheres. The TEM images also showed porous character with a uniform pore diameter and no long-range ordering of these materials (Fig. 5(e) and (f)).

CO_2 uptake capacity analyses of the POSS-F-POIP and POSS-A-POIP were carried out at 298 and 273 K; respectively (Fig. 6(a) and (b)). We found that the POSS-F-POIP and POSS-A-POIP exhibited CO_2 capacities of 1.63 and 1.25 mmol g^{-1}; respectively at 298 K. At 273 K, the CO_2 uptakes of POSS-F-POIP and POSS-A-POIP were 2.28 and 1.8 mmol g^{-1}. The CO_2 uptake performance of the POSS-F-POIP at 298 and 273 K was higher than POSS-A-POIP at the same two temperatures, which are attributed to its high surface area and large pore diameter.

The electrochemical performance of POSS-F-POIP and POSS-A-POIP

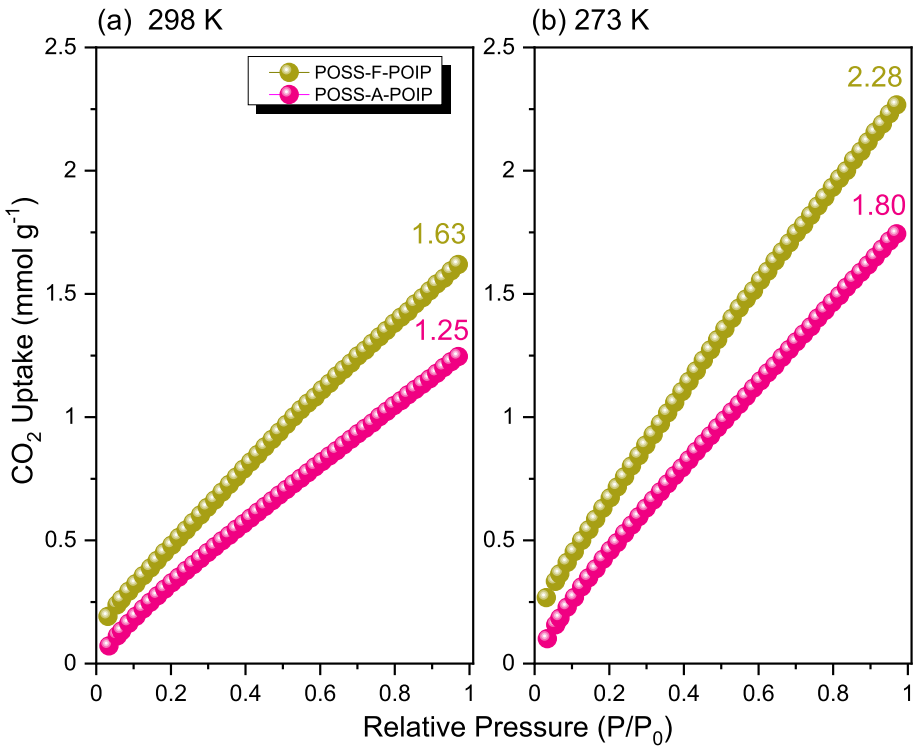

Fig. 6. CO_2 capacities of POSS-F-POIP and POSS-A-POIP were recorded at 298 K (a) and 273 K (b).

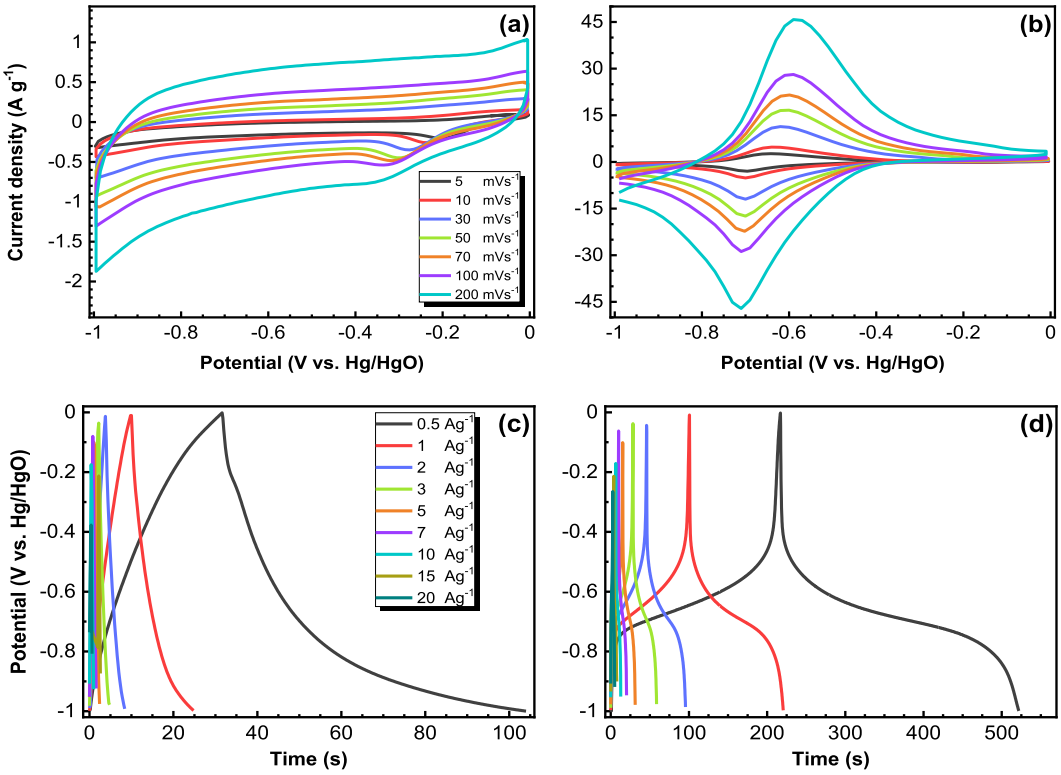

Fig. 7. (a and b) CV and (c and d) GCD profiles, recorded in 1 M KOH of (a and c) POSS- F-PIOP and (b and d) POSS-A-POIP.

samples was estimated through galvanostatic charge-discharge (GCD) and cyclic voltammetry (CV) measurements in 1 M KOH aqueous solution using the three-electrode system. Fig. 7 shows the CV curves of POSS-F-POIP and POSS-A-POIP samples measured at different scan rates of 5–200 mV s^{-1} in the potential window from −1.00 to 0 V (*vs.* Hg/HgO). These CV curves of the POSS-F-POIP sample (Fig. 7(a)) showed rectangular-like shapes with humps, implying that this capacitive response originated from EDLC [66,67]. This appearance of humps in the rectangular-like shape is a sign of pseudocapacitance arising from the existence of the electron-rich phenyl rings and the electroactive

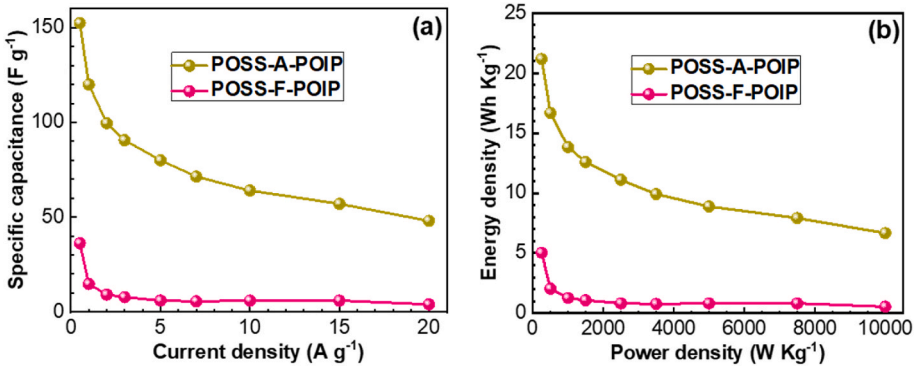

Fig. 8. (a) Corresponding specific capacitances determined at various current densities and (b) Ragone plot of POSS-F-POIP and POSS-A-POIP.

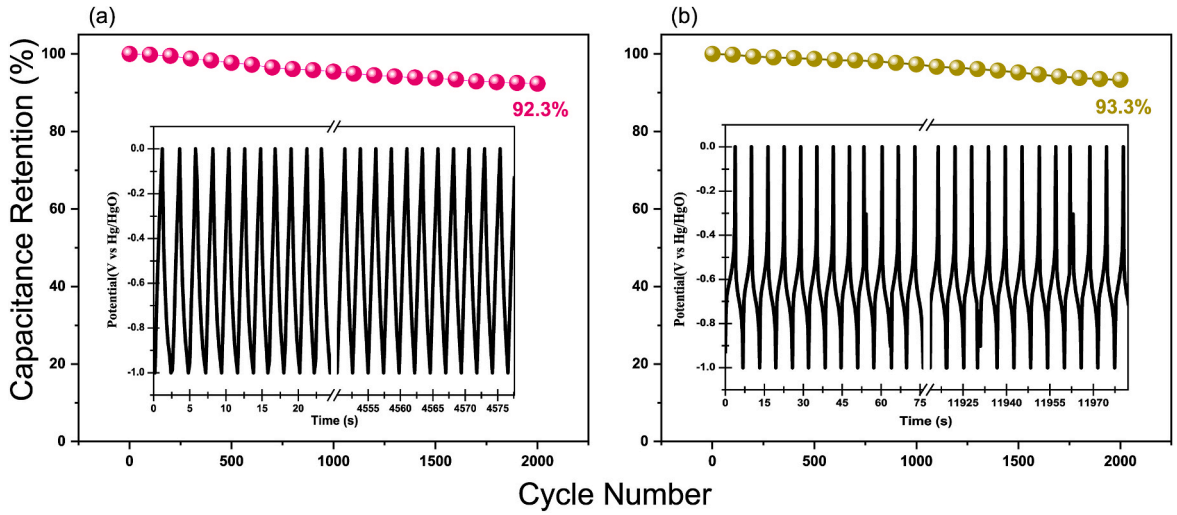

Fig. 9. Cycling stabilities of (a) POSS-F-POIP and (b) POSS-A-POIP, obtained at 10 A g^{-1} after 2000 cycles.

methylene group at position 9 of the fluorene backbone where the redox process occurred during charge and discharge procedures [68]. The anthraquinone backbone within the POSS-A-POIP sample undergoes a reversible redox process, as shown in the voltammetric profile (Fig. 7 (b)). Upon increasing the scan rate from 5 to 200 mV s^{-1}, the shape of CV curves was retained, and the peak current density was increased, suggesting facile kinetics and good electron-transporting properties [69,70]. The peak separation ($\Delta E_p \approx 120\,mV$) between the reduction and oxidation, peaks were relatively small, indicative of fast electron transfer [70,71]. The symmetrical features of redox peaks are an indication of the high reversibility of the redox Reaction. The POSS-A-POIP exhibited a very higher current density compared to the POSS-F-POIP. Fig. 7(c) and (d) present the GCD curves of the POSS-F-POIP and POSS-A-POIP samples, recorded at different current densities of 0.5–20 A g^{-1}. The GCD curves of the POSS-F-POIP sample possess triangular shapes with a slight bend, indicating both EDLC and pseudocapacity characteristics [70,71]. The GCD curves of the POSS-A-POIP sample showed the typical feature of pseudocapacitor with high symmetry, indicating good electrochemical reversibility and capacitance performance [74,75]. The discharging time of the POSS-A-POIP was longer than the POSS-F-POIP (Fig. 7(c) and (d)), implying that the capacitance of the POSS-A-POIP was larger than the POSS-F-POIP. Fig. 8(a) presents the specific capacitances of POSS-F-POIP and POSS-A-POIP samples calculated from GCD curves based on Eq. (S1). The POSS-A-POIP displayed excellent capacitance compared to other porous materials (Table S1), with a value of 152.5 F g^{-1} at the current density of 0.5 A g^{-1}. The excellent performance could be attributed to the Faradaic reaction of anthraquinone and the π-conjugated system. Moreover, the Ragone plot (Fig. 8(b)) showed that the POSS-A-POIP electrode has higher energy and power densities compared with the POSS-F-POIP. The capacitance retention of POSS-F-POIP and POSS-A-POIP were 92.3 and 93.0% after 2000 GCD cycles (Fig. 9). In this regard, DeBlase et al. proposed the DAAQ-TFP COF with the capacitance of ca. 48 F g^{-1} at 0.1 A g^{-1}, which stabilized at ca. 40 F g^{-1} after 10 GCD cycles [70]. Sun et al. synthesized novel nanocomposite of graphene nanosheets/acid-treated multi-walled carbon nanotube-supported poly (1,5-diaminoanthraquinone), this composite exhibited a specific capacitance of 80.8 F g^{-1} at 0.5 A g^{-1}, respectively, in 1 mol L^{-1} tetraethylammonium tetrafluoroborate-acetonitrile (Et_4NBF_4-AN) electrolyte [72]. In addition, Xu et al. prepared flexible 1,4,5,8-tetrahydroxy anthraquinone (THAQ)/graphene composite electrodes (THAQ/rGO) and hydrothermal-treated THAQ (H-THAQ) as a control sample, and the H-THAQ and THAQ/rGO composite showed specific capacitance of 15 and 76 F g^{-1} at 1.00 A g^{-1}, respectively, in 1 M H_2SO_4 solution [73]. Moreover, Guo et al. studied the electrochemical performance of 1, 4-naphthoquinone (AQ) for supercapacitor [71]. The AQ exhibited a specific capacitance of 42 F g^{-1} at 1.00 A g^{-1}. Recently, we proposed that TPE-DDSQ POIP and Car-DDSQ POIP displayed a specific capacitance of 22 and 23 F g^{-1} at 1 A g^{-1} [30]. We also prepared poly(cyanate ester)–functionalized DDSQ and this material had a specific capacitance of 20 F g^{-1} [86]. Also, the POSS-A-POIP exhibited specific capacitances higher than those of conjugated microporous polymers [74], porous organic polymers [66], and covalent organic frameworks [75].

4. Conclusion

Two types of organic-inorganic hybrid porous polymers, POSS-F-POIP and POSS-A-POIP were synthesized simultaneously using cubic polyhedral oligomeric silsesquioxanes (OVS) as building blocks and two different brominated monomers via Heck cross-coupling reactions. According to N_2 isotherm and TGA analyses revealed that POSS-A-POIP had a BET surface area of 426 m^2 g^{-1} and a high T_{d10} up to 600 °C with char yield up to 83 wt%. In addition, the specific capacitance of the POSS-F-POIP and POSS-A-POIP were 36.2 and 152.5 F g^{-1}, respectively. From electrochemical results, the POSS-A-POIP exhibited outstanding energy storage performance compared to POSS-F-POIP and other porous framework materials because of the π-conjugated system and the Faradaic reaction of anthraquinone moiety.

CRediT authorship contribution statement

Mohamed Gamal Mohamed: Investigation, Methodology, Conceptualization, Formal analysis, Writing – original draft, Data curation. **Yasuno Takashi:** Data curation.

Declaration of competing interest

The authors declare that they have no known competing financial interests or personal relationships that could have appeared to influence the work reported in this paper.

Acknowledgments

This study was supported financially by the Ministry of Science and Technology, Taiwan, under contracts MOST 108-2638-E-002-003-MY2, and 108-2221-E-110-014-MY3. The authors thank to the staff at National Sun Yat-sen University for assistance with TEM (ID: EM022600) experiments.

Appendix A. Supplementary data

Supplementary data to this article can be found online at https://doi.org/10.1016/j.micromeso.2021.111505.

References

[1] A. Thomas, Functional materials: from hard to soft porous frameworks, Angew. Chem. Int. Ed. 49 (2010) 8328.
[2] N. Chaoui, M. Trunk, R. Dawson, J. Schmidt, A. Thomas, Trends and challenges for microporous polymers, Chem. Soc. Rev. 46 (2017) 3302–3321.
[3] K.I. Aly, M.M. Sayed, M.G. Mohamed, S.W. Kuo, O. Younis, A facile synthetic route and dual function of network luminescent porous polyester and copolyester containing porphyrin moiety for metal ions sensor and dyes adsorption, Microporous Mesoporous Mater. 298 (2020) 110063.
[4] T. Geng, C. Zhang, G. Chen, L. Ma, W. Zhang, H. Xia, Synthesis of tetraphenylethylene-based fluorescent conjugated microporous polymers for fluorescent sensing and adsorbing iodine, Microporous Mesoporous Mater. 284 (2019) 468–475.
[5] M.G. Mohamed, M.H. Elsayed, A.M. Elewa, A.F.M. EL-Mahdy, C.H. Yang, A.A. K. Mohammed, H.H. Chou, S.W. Kuo, Pyrene-containing conjugated organic microporous polymers for photocatalytic hydrogen evolution from water, Catal. Sci. Technol. 11 (2021) 2229–2241.
[6] C. Dai, L. Zhong, X. Gong, L. Zeng, C. Xue, S. Li, B. Liu, Triphenylamine based conjugated microporous polymers for selective photoreduction of CO_2 to CO under visible light, Green Chem. 21 (2019) 6606–6610.
[7] R.S. Sprick, J.X. Jiang, B. Bonillo, S. Ren, T. Ratvijitvech, P. Guiglion, M. A. Zwijnenburg, D.J. Adams, A.I. Cooper, Tunable organic photocatalysts for visible-light-driven hydrogen evolution, J. Am. Chem. Soc. 137 (2015) 3265–3270.
[8] F. Xu, X. Chen, Z. Tang, D. Wu, R. Fu, D. Jiang, Redox-active conjugated microporous polymers: a new organic platform for highly efficient energy storage, Chem. Commun. 50 (2014) 4788–4790.
[9] J.X. Jiang, F. Su, A. Trewin, C.D. Wood, N.L. Campbell, H. Niu, C. Dickinson, A. Y. Ganin, M.J. Rosseinsky, Y.Z. Khimyak, A.I. Cooper, Conjugated microporous poly(aryleneethynylene) networks, Angew. Chem. Int. Ed. 46 (2007) 8574–8578.
[10] A.I. Cooper, Conjugated microporous polymers, Adv. Mater. 21 (2009) 1291–1295.
[11] M.G. Mohamed, C.C. Lee, A.F.M. EL-Mahdy, J. Lüder, M.H. Yu, Z. Li, Z. Zhu, C. C. Chueh, S.W. Kuo, Exploitation of two-dimensional conjugated covalent organic frameworks based on tetraphenylethylene with bicarbazole and pyrene units and applications in perovskite solar cells, J. Mater. Chem. 8 (2020) 11448–11459.
[12] H.R. Abuzeid, A.F.M. EL-Mahdy, S.W. Kuo, Covalent organic frameworks: design principles, synthetic strategies, and diverse applications, Giant 6 (2021) 100054.
[13] X. Zhang, B. Qiu, Y. Zou, S. Wang, W. Mai, Y. Cao, Y. Wang, J. Chen, T. Li, Green synthesized cobalt-bipyridine constructed conjugated microporous polymer: an efficient heterogeneous catalyst for cycloaddition of epoxides via CO_2 fixation under ambient conditions, Microporous Mesoporous Mater. 319 (2020) 110758.
[14] C. Zhang, Y. He, P. Mu, X. Wang, Q. He, Y. Chen, J. Zeng, F. Wang, Y. Xu, J. X. Jiang, Toward high performance thiophene-containing conjugated microporous polymer anodes for lithium-ion batteries through structure design, Adv. Funct. Mater. 28 (2018) 1705432.
[15] C. Zhang, Y. Qiao, P. Xiong, W. Ma, P. Bai, X. Wang, Q. Li, J. Zhao, Y. Xu, Y. Chen, J.H. Zeng, F. Wang, Y. Xu, J.X. Jiang, Conjugated microporous polymers with tunable electronic structure for high-performance potassium-ion batteries, ACS Nano 13 (2019) 745–754.
[16] K. Amin, N. Ashraf, L. Mao, C.F.J. Faul, Z. Wei, Conjugated microporous polymers for energy storage: recent progress and challenges, Nano Energy 85 (2021) 105958.
[17] F. Vilela, K. Zhang, M. Antonietti, Conjugated porous polymers for energy applications, Energy Environ. Sci. 5 (2012) 7819–7832.
[18] J.S.M. Lee, A.I. Cooper, Advances in conjugated microporous polymers, Chem. Rev. 120 (2020) 2171–2214.
[19] M.G. Mohamed, A.F.M. EL-Mahdy, M.M.M. Ahmed, S.W. Kuo, Direct synthesis of microporous bicarbazole-based covalent triazine frameworks for high-performance energy storage and carbon dioxide uptake, ChemPlusChem 84 (2019) 1767–1774.
[20] R. Vinodh, C.V.V.M. Gopi, V.G.R. Kummara, R. Atchudanc, T. Ahamad, S. Sambasivam, M. Yi, I.M. Obaidat, H.J. Kim, A review on porous carbon electrode material derived from hypercrosslinked polymers for supercapacitor applications, J. Energy Stor. 32 (2020) 101831.
[21] M.G. Mohamed, A.F.M. EL-Mahdy, Y. Takashi, S.W. Kuo, Ultrastable conductive microporous covalent triazine frameworks based on pyrene moieties provide high-performance CO_2 uptake and supercapacitance, New J. Chem. 44 (2020) 8241–8253.
[22] P. Bhanja, S.K. Das, K. Bhunia, D. Pradhan, T. Hayashi, Y. Hijikata, S. Irle, A. Bhaumik, A new porous polymer for highly efficient capacitive energy storage, ACS Sustain. Chem. Eng. 6 (2018) 202–209.
[23] H.G. Wang, Z.H. Cheng, Y.Z. Liao, J.H. Li, J. Weber, A. Thomas, C.F.J. Faul, Conjugated microporous polycarbazole networks as precursors for nitrogen-enriched microporous carbons for CO_2 storage and electrochemical capacitors, Chem. Mater. 29 (2017) 4885.
[24] J.X. Jiang, F. Su, A. Trewin, C.D. Wood, H. Niu, J.T.A. Jones, Y.Z. Khimyak, A. I. Cooper, Synthetic control of the pore dimension and surface area in conjugated microporous polymer and copolymer networks, J. Am. Chem. Soc. 130 (2008) 7710–7720.
[25] M.G. Mohamed, T.C. Chen, S.W. Kuo, Solid-state chemical transformations to enhance gas capture in benzoxazine-linked conjugated microporous polymers, Macromolecules 54 (2021) 5866–5877.
[26] M.G. Mohamed, E.C.A. Jr, B.M. Matsagar, J.B. Na, Y. Yamauchi, K.C.W. Wu, S. W. Kuo, Construction hierarchically mesoporous/microporous materials based on block copolymer and covalent organic framework, J. Taiwan Inst. Chem. Eng 112 (2020) 180–192.
[27] A.F.M. El-Mahdy, M.G. Mohamed, T.H. Mansoure, H.H. Yu, T. Chen, S.W. Kuo, Ultrastable tetraphenyl-p-phenylenediamine-based covalent organic frameworks as platforms for high-performance electrochemical supercapacitors, Chem. Commun. 55 (2019) 14890–14893.
[28] A.F.M. EL-Mahdy, T.C. Yu, M.G. Mohamed, S.W. Kuo, Secondary structures of polypeptide-based diblock copolymers influence the microphase separation of templates for the fabrication of microporous carbons, Macromolecules 54 (2021) 1030–1042.
[29] M. Sachs, R.S. Sprick, D. Pearce, S.A.J. Hillman, A. Monti, A.A.Y. Guilbert, N. J. Brownbill, S. Dimitrov, X. Shi, F. Blanc, M.A. Zwijnenburg, J. Nelson, J. R. Durrant, A.I. Cooper, Understanding structure-activity relationships in linear polymer photocatalysts for hydrogen evolution, Nat. Commun. 9 (2018) 4968.
[30] M.G. Mohamed, W.C. Chen, A.F.M. EL-Mahdy, S.W. Kuo, Porous organic/inorganic polymers based on double-decker silsesquioxane for high-performance energy storage, J. Polym. Res. 28 (2021) 219.
[31] R.S. Sprick, Y. Bai, A.A.Y. Guilbert, M. Zbiri, C.M. Aitchison, L. Wilbraham, Y. Yan, D.J. Woods, M.A. Zwijnenburg, A.I. Cooper, Photocatalytic hydrogen evolution from water using fluorene and dibenzothiophene sulfone-conjugated microporous and linear polymers, Chem. Mater. 2 (2019) 305–313.
[32] M.G. Mohamed, S.M. Ebrahium, A.S. Hammam, S.W. Kuo, K.I. Aly, Enhanced CO_2 capture in nitrogen-enriched microporous carbons derived from Polybenzoxazines containing azobenzene and carboxylic acid units, J. Polym. Res. 27 (2020) 197.
[33] M.M. Samy, M.G. Mohamed, S.W. Kuo, Pyrene-functionalized tetraphenylethylene polybenzoxazine for dispersing single-walled carbon nanotubes and energy storage, Compos. Sci. Technol. 199 (2020) 108360.
[34] W.S. Hung, M.M.M. Ahmed, M.G. Mohamed, S.W. Kuo, Competing hydrogen bonding produces mesoporous/macroporous carbons templated by a high-molecular-weight poly(caprolactone–b–ethylene oxide–b–caprolactone) triblock copolymer, J. Polym. Res. 27 (2020) 173.
[35] M.G. Mohamed, A.F.M. EL-Mahdy, T.S. Meng, M.M. Samy, S.W. Kuo, Multifunctional hypercrosslinked porous organic polymers based on tetraphenylethene and triphenylamine derivatives for high-performance dye adsorption and supercapacitor, Polymers 12 (2020) 2426.

[36] A.M. Elewa, A.F.M. EL-Mahdy, M.H. Elsayed, M.G. Mohamed, S.W. Kuo, H. H. Chou, Sulfur-doped triazine-conjugated microporous polymers for achieving the robust visible-light-driven hydrogen evolution, Chem. Eng. J. 421 (2021) 129825.
[37] W. Ma, C. Zhang, X. Gao, C. Shu, C. Yan, F. Wang, Y. Chen, J.H. Zeng, J.X. Jiang, Structure evolution of azo-fused conjugated microporous polymers for high performance lithium-ion batteries anodes, J. Power Sources 453 (2020) 227868.
[38] J.Y. Wu, M.G. Mohamed, S.W. Kuo, Directly synthesized nitrogen-doped microporous carbons from polybenzoxazine resins for carbon dioxide capture, Polym. Chem. 8 (2017) 5481–5489.
[39] G. Singh, J. Lee, A. Karakoti, R. Bahadur, J. Yi, D. Zhao, K. AlBahily, A. Vinu, Emerging trends in porous materials for CO_2 capture and conversion, Chem. Soc. Rev. 49 (2020) 4360–4404.
[40] M.G. Mohamed, M.M.M. Ahmed, W.T. Du, S.W. Kuo, Meso/microporous carbons from conjugated hyper-crosslinked polymers based on tetraphenylethene for high-performance CO_2 capture and supercapacitor, Molecules 26 (2021) 738.
[41] M.G. Mohamed, M.Y. Tsai, W.C. Su, A.F.M. EL-Mahdy, C.F. Wang, C.F. Huang, L. Dai, T. Chen, S.W. Kuo, Nitrogen-Doped microporous carbons derived from azobenzene and nitrile-functionalized polybenzoxazines for CO_2 uptake, Mater. Today Commun. 24 (2020) 101111.
[42] M.G. Mohamed, W.S. Hung, A.F.M. El-Mahdy, M.M.M. Ahmed, L. Dai, T. Chen, S. W. Kuo, High-Molecular-Weight PLA-b-PEO-b-PLA triblock copolymer templated large mesoporous carbons for supercapacitors and CO_2 capture, Polymers 12 (2020) 1193.
[43] M.M. Samy, M.G. Mohamed, A.F.M. EL-Mahdy, T.H. Mansoure, K.C.W. Wu, S. W. Kuo, High-performance supercapacitor electrodes prepared from dispersions of tetrabenzonaphthalene-based conjugated microporous polymers and carbon nanotubes, ACS Appl. Mater. Interfaces (2021), https://doi.org/10.1021/acsami.1c05720.
[44] D. Wang, W. Yang, L. Li, X. Zhao, S. Feng, H. Liu, Hybrid networks constructed from tetrahedral silicon-centered precursors and cubic POSS-based building blocks via Heck reaction: porosity, gas sorption, and luminescence, J. Mater. Chem. 1 (2013) 13549–13558.
[45] M.G. Mohamed, M.Y. Tsai, C.F. Wang, C.F. Huang, M. Danko, L. Dai, T. Chen, S. W. Kuo, Multifunctional polyhedral oligomeric silsesquioxane (POSS) based hybrid porous materials for CO_2 uptake and iodine adsorption, Polymers 13 (2021) 221.
[46] D. Wang, W. Yang, S. Feng, H. Liu, Amine post-functionalized POSS-based porous polymers exhibiting simultaneously enhanced porosity and carbon dioxide adsorption properties, RSC Adv. 6 (2016) 13749–13756.
[47] D. Wang, L. Xue, L. Li, B. Deng, S. Feng, H. Liu, X. Zhao, Rational design and synthesis of hybrid porous polymers derived from polyhedral oligomeric silsesquioxanes via Heck coupling reactions, Macromol. Rapid Commun. 34 (2013) 861–866.
[48] M.G. Mohamed, N.Y. Liu, A.F.M. EL-Mahdy, S.W. Kuo, Ultrastable luminescent hybrid microporous polymers based on polyhedral oligomeric silsesquioxane for CO_2 uptake and metal ion sensing, Microporous Mesoporous Mater. 311 (2021) 110695.
[49] W. Chaikittisilp, A. Sugawara, A. Shimojima, T. Okubo, Hybrid porous materials with high surface area derived from bromophenylethenyl-functionalized cubic siloxane-based building units, Chem. Eur J. 16 (2010) 6006–6014.
[50] L. Sun, Z. Liang, J. Yu, Octavinylsilsesquioxane-based luminescent nanoporous inorganic–organic hybrid polymers constructed by the Heck coupling reaction, Polym. Chem. 6 (2015) 917–924.
[51] Q. Wang, H. Liu, C. Jiang, H. Liu, Silsesquioxane-based triphenylamine functionalized porous polymer for CO_2, I_2 capture and nitro-aromatics detection, Polymer 186 (2020) 122004.
[52] Y. Du, M. Unno, H. Liu, Hybrid nanoporous materials derived from ladder- and cage-type silsesquioxanes for water treatment, ACS Appl. Nano Mater. 3 (2020) 1535–1541.
[53] Y. Wang, M. Soldatov, Q. Wang, H. Liu, Phosphazene functionalized silsesquioxane-based porous polymers for absorbing I_2, CO_2 and dyes, Polymer 218 (2021) 123491.
[54] D. Wang, L. Li, W. Yang, Y. Zuo, S. Feng, H. Liu, POSS-based luminescent porous polymers for carbon dioxide sorption and nitroaromatic explosives detection, RSC Adv. 4 (2014) 59877–59884.
[55] D. Wang, W. Yang, S. Feng, H. Liu, Constructing hybrid porous polymers from cubic octavinyl silsequioxane and planar halogenated benzene, Polym. Chem. 5 (2014) 3634–3642.
[56] M.G. Mohamed, S.W. Kuo, Functional silica and carbon nanocomposites based on polybenzoxazines, Macromol. Chem. Phys. 220 (2019) 1800306.
[57] Y. Du, H. Liu, Cage-like silsesquioxanes-based hybrid materials, Dalton Trans. 49 (2020) 5396–5405.
[58] M. Soldatov, H. Liu, Hybrid porous polymers based on cage-like organosiloxanes: synthesis, properties and applications, Prog. Polym. Sci. 119 (2021) 101419.
[59] M.G. Mohamed, S.W. Kuo, Functional polyimide/polyhedral oligomeric silsesquioxane nanocomposites, Polymers 11 (2019) 26.
[60] X. Zhang, S. Zhao, M.G. Mohamed, S.W. Kuo, Z. Xin, Crystallization behaviors of poly (ethylene terephthalate) (PET) with monosilane isobutyl-polyhedral oligomeric silsesquioxanes (POSS), J. Mater. Sci. 55 (2020) 14642–14655.
[61] W.C. Chen, S.W. Kuo, Ortho-imide and allyl groups effect on highly thermally stable polybenzoxazine/double-decker-shaped polyhedral silsesquioxane hybrids, Macromolecules 51 (2018) 9602–9612.
[62] X. Zhang, S. Zhao, S.W. Kuo, W.C. Chen, M.G. Mohamed, Z. Xin, An effective nucleating agent for isotactic polypropylene (iPP): zinc bis- (nadic anhydride) double-decker silsesquioxanes, Polymer 220 (2021) 123574.
[63] M. Soldatov, H. Liu, A POSS-phosphazene based porous material for adsorption of metal ions from water, Chem. Asian J. 14 (2019) 4345–4351.
[64] D. Wang, S. Feng, H. Liu, Fluorescence-tuned polyhedral oligomeric silsesquioxane-based porous polymers, Chem. Eur J. 22 (2016) 14319–14327.
[65] R. Sun, S. Feng, D. Wang, H. Liu, Fluorescence-tuned silicone elastomers for multicolored MOUltraviolet light-emitting diodes: realizing the processability of polyhedral oligomeric silsesquioxane-based hybrid porous polymers, Chem. Mater. 30 (2018) 6370–6376.
[66] M.G. Mohamed, X. Zhang, T.H. Mansoure, A.F.M. El-Mahdy, C.F. Huang, M. Danko, Z. Xin, S.W. Kuo, Hypercrosslinked porous organic polymers based on tetraphenylanthraquinone for CO_2 uptake and high-performance supercapacitor, Polymer 205 (2020) 122857–122866.
[67] A.F.M. El-Mahdy, M.G. Mohamed, T.H. Mansoure, H.H. Yu, T. Chen, S.W. Kuo, Ultrastable tetraphenyl-p-phenylenediamine-based covalent organic frameworks as platforms for high-performance electrochemical supercapacitors, Chem. Commun. 55 (2019) 14890–14893.
[68] X. He, X. Xie, J. Wang, X. Ma, Y. Xie, J. Gu, N. Xiao, J. Qiu, From fluorene molecules to ultrathin carbon nanonets with an enhanced charge transfer capability for supercapacitors, Nanoscale 11 (2019) 6610–6619.
[69] A.M. Khattak, Z.A. Ghazi, B. Liang, N.A. Khan, A. Iqbal, L. Li, Z. Tang, A redox-active 2D covalent organic framework with pyridine moieties capable of faradaic energy storage, J. Mater. Chem. A. 4 (2016) 16312–16317.
[70] C.R. DeBlase, K.E. Silberstein, T.T. Truong, H.D. Abruña, W.R. Dichtel, β-Ketoenamine-Linked covalent organic frameworks capable of pseudocapacitive energy storage, J. Am. Chem. Soc. 135 (2013) 16821–16824.
[71] B. Guo, Y. Yang, Z. Hu, Y. An, Q. Zhang, X. Yang, X. Wang, H. Wu, Redox-active organic molecules functionalized nitrogen-doped porous carbon derived from metal-organic framework as electrode materials for supercapacitor, Electrochim. Acta 223 (2017) 74–84.
[72] M.Q. Sun, G.C. Wang, C.Y. Yang, H. Jiang, C.Z. Li, A graphene/carbon nanotube@π-conjugated polymer nanocomposite for high-performance organic supercapacitor electrodes, J. Mater. Chem. 3 (2015) 3880–3890.
[73] L. Xu, R. Shi, H. Li, C. Han, M. Wu, C.P. Wong, F. Kang, B. Li, Pseudocapacitive anthraquinone modified with reduced graphene oxide for flexible symmetric all-solid-state supercapacitors, Carbon 127 (2018) 459–468.
[74] A.M. Khattak, H. Sin, Z.A. Ghazi, X. He, B. Liang, N.A. Khan, H.R. Alanagh, A. Iqbal, L. Li, Z. Tang, Controllable fabrication of redox-active conjugated microporous polymers on reduced graphene oxide for high performance faradaic energy storage, J. Mater. Chem. 6 (2018) 18827–18832.
[75] A.F.M. El-Mahdy, C.H. Kuo, A. Alshehri, C. Young, Y. Yamauchi, J. Kim, S.W. Kuo, Strategic design of triphenylamine- and triphenyltriazine-based two-dimensional covalent organic frameworks for CO_2 uptake and energy storage, J. Mater. Chem. 6 (2018) 19532–19541.
[76] V. Augustyn, P. Simon, B. Dunn, Pseudocapacitive oxide materials for high-rate electrochemical energy storage, Energy Environ. Sci. 7 (2014) 1597–1614.
[77] J.G. Li, P.Y. Lee, M.M.M. Ahmed, M.G. Mohamed, S.W. Kuo, Varying the hydrogen bonding strength in phenolic/PEO-b-PLA blends provides mesoporous carbons having large accessible pores suitable for energy storage, Macromol. Chem. Phys. 221 (2020) 2000040.
[78] M.M. Samy, M.G. Mohamed, S.W. Kuo, Directly synthesized nitrogen-and-oxygen–doped microporous carbons derived from a bio-derived polybenzoxazine exhibiting high-performance supercapacitance and CO_2 uptake, Eur. Polym. J. 138 (2020) 109954.
[79] M. Jia, Y. Li, L. Cui, Y. An, C. Pan, X. Jin, An anthraquinone-decorated graphene hydrogel based on carbonized cotton fibers for flexible and high performance supercapacitors, Sustain. Energy Fuels 5 (2021) 862–873.
[80] B. Guo, Z. Hu, Y. An, N. An, P. Jia, Y. Zhang, Y. Yang, Z. Li, Nitrogen-doped heterostructure carbon functionalized by electroactive organic molecules for asymmetric supercapacitors with high energy density, RSC Adv. 6 (2016) 40602–40614.
[81] Y. Zhao, Z. Zhao, M. Wei, X. Jiang, H. Li, J. Gao, L. Hou, Preparation of Si-doped and cross-linked carbon nanofibers via electrospinning and their supercapacitive properties, Prog. Nat. Sci.: Met. Mater. Int. 28 (2018) 337–344.
[82] X. Du, Q. Chen, C. Xiang, Y. Zou, F. Xu, J. Xie, L. Sun, formation of highly dispersed ultrafine MnO_2 nanoparticles on nitrogen-doped porous carbon for supercapacitor applications, Int. J. Electrochem. Sci. 14 (2019) 4195–4205.
[83] M.S. Goh, M. Pumera, Multilayer graphene nanoribbons exhibit larger capacitance than their few-layer and single-layer graphene counterparts, Electrochem. Commun. 12 (2010) 1375–1377.
[84] S. Guo, W. Wang, C. Ozkan, M. Ozkan, Assembled graphene oxide and single-walled carbon nanotube ink for stable supercapacitors, J. Mater. Res. 28 (2013) 918–926.
[85] J. Yan, J.H. Choi, Y.G. Jeong, Freestanding supercapacitor electrode applications of carbon nanofibers based on polyacrylonitrile and polyhedral oligomeric silsesquioxane, Mater. Des. 139 (2018) 72–80.
[86] W.C. Chen, M.M.M. Ahmed, C.F. Wang, C.F. Huang, S.W. Kuo, Highly thermally stable mesoporous poly(cyanate ester) featuring double-decker–shaped polyhedral silsesquioxane framework, Polymer 185 (2019) 121940.